Journal of Statistical Physics, Vol. 81, Nos. 1/2, 1995

A New Class of Gas-Kinetic Relaxation Schemes for the Compressible Euler Equations

Kun Xu[1]

Received September 1, 1994; final December 23, 1994

Starting from the gas-kinetic model, a new class of relaxation schemes for the Euler equations is presented. In contrast to the Riemann solver, these schemes provide a multidimensional dynamical gas evolution model, which combines both Lax–Wendroff and kinetic flux vector splitting schemes, and their coupling is based on the fact that a nonequilibrium state will evolve into an equilibrium state along with the increase of entropy. The numerical fluxes are constructed without getting into the details of the particle collisions. The results for many well-defined test cases are presented to indicate the robustness and accuracy of the current scheme.

KEY WORDS: Gas-kinetic relaxation schemes; compressible Euler equations.

1. INTRODUCTION

Many high-resolution shock-capturing schemes have been developed in the past 20 years. Most of them either attempt to resolve wave interactions through the upwind biasing of the discretization or explicitly introduce numerical viscosity in just the amount needed to resolve discontinuities.[6] Generally, there are different design principles for the construction of high-resolution schemes, such as Jameson's symmetric limited positive (SLIP) formulations.[7] The following analysis is similar to van Leer's terminology,[17] but with a different viewpoint, which contains more physical intuition rather than mathematical manipulation.

A high-resolution scheme usually consists of two parts, the reconstruction of the initial data and the dynamical evolution started from the

[1] Department of Mechanical and Aerospace Engineering, Princeton University, Princeton, New Jersey 08544.

0022-4715/95/1000-0147$07.50/0

constructed data. In other words, these two stages can be regarded as geometrical and dynamical correlations for the gas flow around an artificially defined cell boundary.

The geometrical stage is a kinematic description of the flow variables, which tries to recover the continuous physical reality from the discretized data. Caution should be taken whenever doing the interpolations, otherwise Gibbs phenomena or local extrema can be unphysically created. The inclusion of some kind of limiters to eliminate the creation of any local extrema or to restrict the large subcell variations is physically correct and numerically necessary. The interpolated quantities could be continuous or discontinuous at the cell boundary according to the real flow situations; both cases are equally important. The behavior of different limiters is usually problem dependent: one limiter which is good for one test case may show unfavorable results for another one. It seems rather pointless to indulge in this variation of the limiters without good motives. However, using a high-order interpolation does not guarantee that the final scheme will also have the same order of accuracy as the order of the interpolation, since obtaining the solutions of the model equations (such as the Euler equations) with the interpolated data as the initial condition is still questionable.

The second stage is the dynamical correlation, which uses physical models to construct the gas evolution picture starting from the interpolated data, and finally to obtain the numerical fluxes at a cell boundary. For the Euler equations, due to the complicated nonlinear wave interaction, the exact solution can be found only for simple initial value problems. For example, the Riemann solver is an exact solution under the condition of two constant states in the left and right sides of a cell boundary for 1D gas flow. Godunov-type schemes are based on this solution.[3] One advantage of the Godunov method is that it includes dynamical interactions in the gas evolution process, and flow correlations can be clearly observed from the approximate Riemann solver, such as Roe's scheme, where Roe's average is actually some kind of correlation of the flow variables from both sides of a cell boundary.[13] However, except under special physical situations, the real flow distributions are not necessarily two constant states. Thus, the Riemann solver is actually a first-order representation of gas dynamical evolution, and the reconstructed data from the first stage have to be abandoned in some way in order to fit the initial value condition of the Riemann solver. Most authors, however, ignore this point, by mixing the order of the interpolation with the order of dynamics.[17] For example, van Leer points out that all one needs to do to raise the order of accuracy of the upwind differencing scheme is to raise the order of accuracy of the initial value interpolation that yields the zone-boundary data. Although

Godunov-type methods have been successfully used in many numerical calculations, the ability of this gas evolution model to approximate all kinds of physical processes is still doubtful, especially for multidimensional flows. In order to compensate for the limitation of the Riemann solver to represent dynamical gas interaction, Colella and Woodward incorporated more physical reality into their PPM scheme, where two constant states for the Riemann solver are reconstructed from the initially interpolated parabolic distribution according to the local wave speeds, although finding the optimal waves is also a difficult job for the gas dynamical equations.[2]

A numerical scheme should have both the geometrical correlation in the first stage and the dynamical correlation in the second stage, and these two stages are inseparable. The upwind property is best understood when applied to the simple advection equation, where the geometrical and dynamical correlations look the same. For a nonlinear system, such as the Euler equations, the story is different. The main theoretical obstacle to handling all conservation laws by one single method based on the linear advection equation is the need to account for all possible modes of nonlinear interactions, which seems extremely difficult and physically unreasonable. One group of upwind schemes is flux vector splitting (FVS); these schemes are usually excessively diffusive and smear the shear layers.[15, 16] The reason for this is that FVS does not incorporate any dynamical wave interactions between the left- and right-moving waves, or, more precisely, its dynamical evolution model is equivalent to solving the collisionless Boltzmann equation. In this case, the flow variables at the cell boundary can be approximated by a gas distribution function of two half Maxwellians, which have intrinsic viscosity and heat conductivity due to the deviation of its distribution from a real Maxwellian regardless of how much the mesh is refined.[22] There are many versions of flux vector splitting schemes, both for the Euler and gas-kinetic equations. In all these versions, if correlations between the left- and right-moving waves are missed at the dynamical stage, then these schemes will definitely fail for the Navier–Stokes simulations. On the contrary, flux difference splitting (FDS) schemes are less diffusive due to their dynamical wave correlation, therefore the resolution of the shear layers is much better than the FVS schemes.

The advection upstream splitting method of Liou and Steffen is a scheme which fits neither in an FDS framework nor in an FVS framework,[10] but it indeed has the correlations of the left and right states in the construction of common flow variables at cell boundaries through Roe's or other kinds of averages. Hence, it does an extremely good job of resolving the shear layers. But in common with other schemes that use Roe's average, it shows excessive oscillations in the post-shock regions for blunt-body calculations, or even converges to nonphysical solutions under some

extreme conditions due to the flaws in the Roe's average. For example, certain conditions could exist for which Roe-average eigenvalues might lie outside the range determined by the left and right states.[18] Searching for better averages (or dynamical flow correlation) for the left and right states at a cell boundary is still under intensive investigation. For central difference schemes with explicit artificial dissipation, flow correlations are usually obtained by the simple average of the flow variables from both sides of a cell boundary, such as the construction of the matrix $A_{i+1/2}$ in the Lax–Wendroff-type schemes and evaluation of the Euler fluxes in JST schemes.[8] This simple average does not necessarily recover flow dynamical processes, especially in discontinuous regions.

The current state-of-the-art design principles are referred to as total variation diminishing (TVD), essentially nonoscillation (ENO), and local extremum diminishing (LED),[4–6] which are mostly understood for the scalar conservation laws and can be applied reasonably in the interpolation stages. In the gas evolution stage, the solution is not necessarily a decreasing function of time, and local extrema can be physically generated due to the nonlinear wave interactions.

In summary, due to the complicated nature of the Euler equations, only a few solutions can be constructed under very simple initial value conditions, such as the Riemann solver. Fortunately, the dynamical model for the gas evolution is not unique. From the gas-kinetic BGK model,[12, 21, 22] without getting into the details of the particle collisions, the time-dependent solution of the gas distribution function at a cell boundary has been obtained under more flexible initial conditions, where all slopes in x, y, and z directions can be included for the 3D flux calculation. Although how to define the multidimensional interpolation is still uncertain, the dynamical gas evolution model presented in this paper does have multidimensional properties. Also, the intrinsic physical property of upwinding is satisfied on the level of particle motion instead of picking up a limited number of waves. In addition, the numerical solution satisfies the entropy condition naturally.[22] It is known that the BGK model is equivalent to the Euler and Navier–Stokes equations. Therefore, philosophically, developing a scheme from the gas-kinetic model is similar to these approaches of solving the Euler equations, which change its conservative variables into primitive variables in order to get a simple solution, or to figure out a clear physical picture under the new formulation.

Section 2 describes the construction of a new gas evolution model for the compressible Euler equations. In contrast to previous work, the collision time need not appear in the final flux formulation, and the time evolution process is much simplified compared to the original schemes.[12, 21, 22] Following this model, a class of new relaxation schemes can be con-

structed. Section 3 describes the application of the scheme to well-defined test cases.

2. GAS-KINETIC RELAXATION SCHEMES

The fundamental task for constructing a finite-volume gas-kinetic scheme is to evaluate the gas distribution function f at a cell interface, from which the numerical fluxes can be computed. Due to the intrinsic difficulties related to the collision term in the full Boltzmann equation, simplified gas-kinetic models are usually used for studying gas flow problems. Actually, for hydrodynamic simulations, the behavior of the fluid depends very little on the nature of individual particles in that fluid. The most important criterion for the microscopic model is that it satisfies the minimum requirements of conservation laws and symmetries. The collision model used in this paper is the BGK model,[1] from which the Euler and Navier–Stokes equations can be obtained. A group of gas-kinetic schemes based on this model have been developed in the past few years.[12, 21, 22] In this section, a new class of gas relaxation schemes will be presented.

In two dimensions, the BGK model describes the evolution of the gas distribution function f as

$$f_t + uf_x + vf_y = (g - f)/\tau \tag{1}$$

where g is the equilibrium state which the real gas distribution function f approaches in a time scale τ. The collision time τ is usually regarded as a function of local density and temperature. In the above equation, both f and g are function of space (x, y), time t, particle velocity (u, v), and the internal variable ξ (with K degrees of freedom). The relation between the macroscopic mass ρ, momentum P, and energy ε densities with the distribution function f is

$$\begin{pmatrix} \rho \\ P_x \\ P_y \\ \varepsilon \end{pmatrix} = \int \psi_\alpha f \, d\Xi, \qquad \alpha = 1, 2, 3, 4 \tag{2}$$

where ψ_α is the vector of the moment, defined as

$$\psi_\alpha = (1, u, v, \tfrac{1}{2}(u^2 + v^2 + \xi^2)) \tag{3}$$

and $d\Xi = du\, dv\, d\xi$ is the phase-space volume element. In the BGK model, the equilibrium state g has a Maxwellian distribution given by

$$g = Ae^{-\lambda((u-U)^2 + (v-V)^2 + \xi^2)} \tag{4}$$

Here U and V are average macroscopic velocities, and λ is related to the particle mass m and temperature T through $\lambda = m/2kT$. Since mass, momentum, and energy are conservative quantities in the process of particle collisions, f and g have to satisfy the conservation constraint of

$$\int \psi_\alpha (f-g)\, d\Xi = 0, \qquad \alpha = 1, 2, 3, 4 \tag{5}$$

at any point in space and time.

The general integral solution of the BGK model in two dimensions can be written as[9]

$$f(x, y, t, u, v, \xi) = \frac{1}{\tau}\int_0^t g(x', y', t, u, v, \xi)\, e^{-(t-t')/\tau}\, dt' + e^{-t/\tau} f_0(x-ut, y-vt) \tag{6}$$

where $x' = x - u(t-t')$ and $y' = y - v(t-t')$ are the trajectories of particle motion, and f_0 is the gas distribution function f at the beginning of each time step ($t=0$). The final distribution function f at the cell interface (x, y) and time t is determined by two unknown functions of g and f_0. In the following presentation, the center of a cell boundary will be assumed to be at $(x=0,\ y=0)$, and the final numerical fluxes will be evaluated in the x direction.

Considering a smooth 2D gas flow, we can approximate the equilibrium state g around a cell boundary as

$$g = g_0(1 + ax + by + \bar{A}t) \tag{7}$$

where g_0 is a Maxwellian distribution located at $(x=0,\ y=0,\ t=0)$, and a, b, and $\bar{A}$ are Taylor expansions of a Maxwellian which have the following form:

$$\begin{aligned} a &= a_1 + a_2 u + a_3 v + a_4(u^2 + v^2 + \xi^2) \\ b &= b_1 + b_2 u + b_3 v + b_4(u^2 + v^2 + \xi^2) \\ \bar{A} &= \bar{A}_1 + \bar{A}_2 u + \bar{A}_3 v + \bar{A}_4(u^2 + v^2 + \xi^2) \end{aligned} \tag{8}$$

All parameters of $a_1, a_2, \ldots, \bar{A}_4$ are local constants. These constants A, λ, U, and V in g_0 can be obtained directly from the interpolated macroscopic variables at a cell boundary or from the assumption of f_0, as shown later. Then, a and b can be found from the slopes of the initial interpolations of macroscopic mass, momentum, and energy densities across the cell boundary at time $t=0$. In smooth flow regions, the initial gas distribution

f_0 usually stays in an equilibrium state, which is equal to g at $t=0$. Under this assumption, we have

$$f_0 = g_0(1 + ax + by) \tag{9}$$

Substituting both Eqs. (9) and (7) into Eq. (6), we can obtain the time-dependent f at the cell boundary

$$f = g_0(1 + \tau(-1 + e^{-t/\tau})(ua + vb) + \tau(t/\tau - 1 + e^{-t/\tau})\,\bar{A}) \tag{10}$$

In order to obtain the unknown term $\bar{A}$ in the above equation, the compatibility condition, Eq. (5), has to be used. The expression of $f-g$ at the cell boundary is

$$f - g = g_0\tau(-1 + e^{-t/\tau})(ua + vb + \bar{A}) \tag{11}$$

which determines $\bar{A}$ solely from its moments in terms of the moments of a and b,

$$\int \psi_\alpha g_0 \bar{A}\, d\Xi = -\int \psi_\alpha g_0(au + vb)\, d\Xi \tag{12}$$

The above relation guarantees that the compatibility condition, Eq. (5), is satisfied exactly at any time within the whole time step. In previous work[12, 21, 22] the averaging of this condition over the whole time step was used to evaluate $\bar{A}$. The technique of obtaining $\bar{A}$ in Eq. (12) is similar to the Lax–Wendroff scheme. However, the matrix transformation that connects space and time derivatives is easier to evaluate from the above gas-kinetic description than that usually used in the Lax–Wendroff-type schemes, especially for the Navier–Stokes equations. The nonlinear formulation of the Lax–Wendroff scheme requires the evaluation of the Jacobian matrix $A_{i+1/2}$ at the cell boundary, and the matrix here is a function of g_0 in the current gas-kinetic scheme. As we will show later for the evaluation of g_0, the gas-kinetic approach leads to an alternative, nonlinear variant of the basic Lax–Wendroff schemes. In a region of smooth flow, f in Eq. (10) is an accurate representation of the gas distribution function for the Navier–Stokes solutions.[20]

For real gas flows, due to the nonlinearity of the BGK model, shock waves whose scales are smaller than the cell size are easily formed. In these regions, the initial gas distribution function f_0 is a dramatically spatially varying function and remains in a nonequilibrium state. So, a safe representation of f_0 around a cell interface is to interpolate it in the $x>0$ and

$x<0$ regions separately. Thus, instead of Eq. (9), in the simplest case (ignoring higher order terms), we can assume f_0 to be discontinuous,

$$f_0=\begin{cases} g^l, & x<0 \\ g^r, & x>0 \end{cases} \tag{13}$$

Both g^l and g^r are Maxwellians, which can be obtained from the interpolations of the initial macroscopic mass, momentum, and energy densities at both sides of a cell boundary. Limiters should be involved in this interpolation stage. Substituting f_0 into Eq. (6) and taking the limit as $t\to 0$, one finds that f should approach f_0 at $x=0$, with

$$f=f_0|_{x=0}=\begin{cases} g^l, & u>0 \\ g^r, & u<0 \end{cases} \tag{14}$$

Because the nonequilibrium state f_0 and the equilibrium state g_0 have to satisfy the conservation constraint (5) at ($x=0$, $y=0$, $t=0$), then g_0 in Eq. (7) can be obtained in the following way,

$$\begin{aligned} \int_{-\infty}^{+\infty} \psi_\alpha g_0\, d\Xi &= \int_{-\infty}^{+\infty} \psi_\alpha f_0\, d\Xi \\ &= \int_{u>0} \psi_\alpha g^l\, d\Xi + \int_{u<0} \psi_\alpha g^r\, d\Xi, \qquad \alpha=1,2,\ldots,4 \end{aligned} \tag{15}$$

The construction of g_0 in Eq. (15) gives a new way to construct flow variables at a cell boundary, and this construction is unique for the gas-kinetic scheme. Also, it can be shown that the entropy of g_0 is always larger than the entropy of f_0 in the above construction,[22] which guarantees that the dynamical system evolves in a physically correct direction. The underlying assumption for this construction is that gas particles from the left and right sides will collapse totally and instantaneously at the cell boundary to form an equilibrium state. This assumption creats "pseudocollisions" in the gas flow at the cell boundary, which prevents the particles from penetrating each other easily, and these "pseudocollisions" also provide additional artificial viscosity, which could probably poison the real physical viscosity in the Navier–Stokes equations. For the Euler calculations, however, the advantage of this assumption is that it could increase the stability region for the numerical calculation and reduce numerical noise in the results. But, physically, this assumption is too restrictive for a real flow problem, especially for shock waves, where a dissipative, nonequilibrium, and stable structure could exist without relaxing into an equilibrium state. Fortunately, the resulting g_0 in the above equation is an imaginary equilibrium

state, and the BGK model only tells us that the real gas distribution f will approach g_0, but it is not necessarily equal to it. With the assumption of $g = g_0(1 + ax + by + \bar{A}t)$ in Eq. (7) and f_0 in Eq. (14), to the order of the Euler equations, the resulting gas distribution function f at a cell boundary can be approximated as

$$f(0, 0, 0, t) = (1 - e^{-t/\tau})\, g_0 t \bar{A} g_0 + e^{-t/\tau} f_0 \tag{16}$$

The above equation describes a relaxation process for the nonequilibrium state f_0 evolving into the equilibrium state g_0. At the same time, due to the spatial variation of macroscopic variables across the cell boundary, the equilibrium state is also a time-evolving function. The time-dependent term $\bar{A}$ not only increases the time step for the numerical simulations, but also gives a high order of accuracy for unsteady flow calculations. Equation (16) can be arranged as

$$f(0, 0, 0, t) = g_0(1 + \bar{A}t) + e^{-t/\tau}(f_0 - g_0) \tag{17}$$

In contrast to the Riemann solver, the above equation describes a multi-dimensional dynamical gas evolution model, which provides the time-dependent gas distribution function at a cell boundary. The first term in the right-hand side of Eq. (17) is the gas-kinetic Lax–Wendroff scheme, which accounts for the time evolution of the equilibrium gas distribution function. The second one is the gas-kinetic dissipation term, which is proportional to the differences between the nonequilibrium and equilibrium states. For example, the shock wave is a dissipative and stable system, which is far away from an equilibrium state. In this case, the second term should be large. However, flux vector splitting and kinetic flux vector splitting schemes usually overemphasize the nonequilibrium property of the gas distribution.[15, 16, 11] Instead of Eq. (17), they use $f = f_0$ as the distribution function at the cell boundary to evaluate the numerical fluxes. Therefore, FVS schemes are very dissipative due to the two half Maxwellians in f_0 [Eq. (14)].

Equation (17) can be integrated directly to get time-dependent numerical fluxes, along with the modification of the collision time.[21, 12, 22] But in order to simplify further the gas relaxation process for the Euler calculations, $e^{-t/\tau}$ will be approximated by simple physical models. Generally, we can rewrite Eq. (17) as

$$f(0, 0, 0, t) = g_0(1 + \bar{A}t) + \mathscr{L}(\cdot)(f_0 - g_0) \tag{18}$$

where $\mathscr{L}(\cdot)$ is the relaxation parameter, and should be a function of local flow variables. $\mathscr{L}(\cdot)$ determines how fast the system can be evolving into the equilibrium state.

There are many ways to construct $\mathscr{L}(\cdot)$. In this paper one choice of $\mathscr{L}(\cdot)$ is given. As we know, for shock waves, the distribution function will stay in a nonequilibrium state along with the pressure jumps across the shock. So, the function $\mathscr{L}(\cdot)$ can be designed as a function of local pressure differences around the cell boundary $(i+1/2)$, as

$$\mathscr{L}(\cdot) = 1 - e^{-C_0 \max(\Delta p_1, \Delta p_2)} \tag{19}$$

where

$$\Delta p_1 = \frac{|(p_{i-1,j} + p_{i+1,j} - 2p_{i,j})|}{|p_{i,j} - p_{i-1,j}| + |p_{i+1,j} - p_{i,j}|} \tag{20}$$

$$\Delta p_2 = \frac{|(p_{i,j} + p_{i+2,j} - 2p_{i+1,j})|}{|p_{i+1,j} - p_{i,j}| + |p_{i+2,j} - p_{i+1,j}|} \tag{21}$$

The new scheme presented in this section will be summarized as follows. From the interpolation of macroscopic conservative variables, according to Eq. (13), f_0 is constructed, from which g_0 can be obtained [Eq. (15)]. After this, a and b in Eq. (7) are found from the differences of the macroscopic variables across the cell boundary $(i+1/2)$, such as $p_{i+1,j} - p_{i,j}$. Then, from Eq. (12), $\bar{A}$ is obtained in terms of a and b. Finally, the distribution function at the cell boundary is f in Eq. (18), where the relaxation parameter $\mathscr{L}(\cdot)$ is determined by Eq. (19). The numerical fluxes across the cell boundary at $(i+1/2)$ in the x direction are given by

$$\mathscr{F}_\alpha = \int \psi_\alpha u f(0, 0, t)\, d\Xi \tag{22}$$

After the integration in the above formula, there are no microscopic variables involved in the numerical fluxes. Then, the evolution of mass, momentum, and energy densities in the x direction in cell j in a time step from t^n to t^{n+1} is

$$\begin{pmatrix} \rho \\ P_x \\ P_y \\ \varepsilon \end{pmatrix}_j^{n+1} = \begin{pmatrix} \rho \\ P_x \\ P_y \\ \varepsilon \end{pmatrix}_j^{n} + \int_0^{\Delta t} (\mathscr{F}_\alpha)_{j-1/2}\, dt - \int_0^{\Delta t} (\mathscr{F}_\alpha)_{j+1/2}\, dt, \quad \alpha = 1, 2, 3, 4 \tag{23}$$

where $\Delta t = t^{n+1} - t^n$ is the time step, and $j-1/2$ and $j+1/2$ are the left and right cell boundaries, respectively, for cell j.

3. NUMERICAL EXAMPLES

Many 1D and 2D test cases have been presented for the numerical Euler and Navier–Stokes solutions using the earlier gas-kinetic schemes based on the solution of the BGK model.[12, 21, 22] It appears that this scheme can give an accurate result for problems with a strong rarefaction wave in the high-speed, low-density regions. Actually, this is not surprising, since all particles with velocities from $-\infty$ to $+\infty$ have been considered in the process of computing numerical fluxes.

In all the following, we will apply the new scheme developed in this paper to some well-known test cases with strong shocks. In all calculations, the van Leer limiter

$$L(u, v) = S(u, v)\frac{2|u| \cdot |v|}{|u| + |v|} \tag{24}$$

with $S(u, v) = 1/2\{\text{sign}(u) + \text{sign}(v)\}$, is used for the interpolations of the macroscopic variables in order to construct f_0, and $C_0 = 1.0$ is used in Eq. (19).

Case 1. The classical Sod test case is a shock-tube problem, which has the initial conditions $\rho_l = 1$, $P_l = 0$, $\varepsilon_l = 2.5$ and $\rho_r = 0.125$, $P_r = 0$, $\varepsilon_r = 0.25$. Our results for 200 points are shown in Fig. 1, where the solid line is the exact solutions.[14]

Case 2. The second test case is the blast-wave test with the initial conditions $\rho_l = 1.0$, $P_l = 0$, $\varepsilon_l = 2500$ for $0 < x \leqslant 0.1$, $\rho_m = 1.0$, $P_m = 0.0$, $\varepsilon_m = 0.025$ for $0.2 < x \leqslant 0.9$; and $\rho_r = 1.0$, $P_r = 0.0$, $\varepsilon_r = 250$ for $0.9 < x \leqslant 1$.[19]. We used 400 points in this case, and the results are shown in Fig. 2, where the solid lines are obtained from the same scheme with 800 points.

Case 3. The forward-facing step test is carried out on a uniform mesh of 240×80 cells.[19] The density distribution is shown in Fig. 3. In contrast to the original Woodward and Colella calculations, there is no special treatment around the corner in this case, and the second Mach stem is much shorter than most results obtained from other shock-capturing schemes.

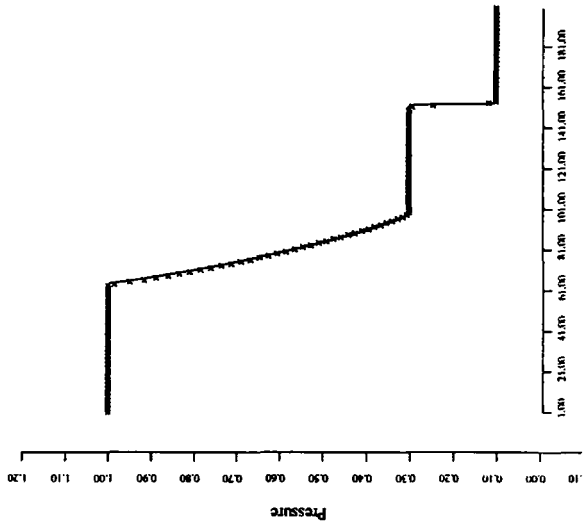
Pressure
0.00
0.10
0.20
0.30
0.40
0.50
0.60
0.70
0.80
0.90
1.00
1.10
1.20
1.00
21.00
41.00
61.00
81.00
101.00
121.00
141.00
161.00
181.00

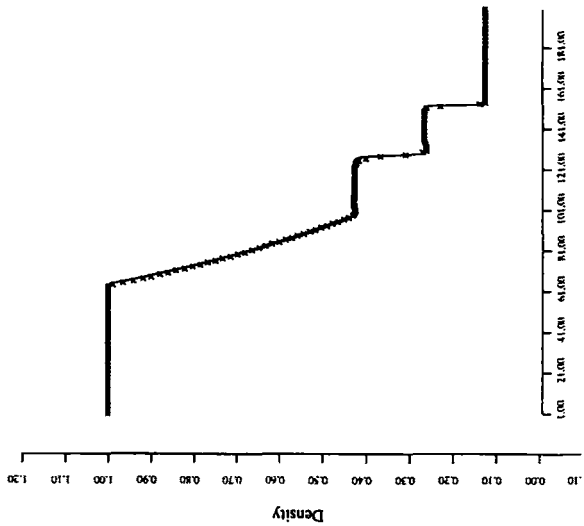
Density
0.00
0.10
0.20
0.30
0.40
0.50
0.60
0.70
0.80
0.90
1.00
1.10
1.20
1.00
21.00
41.00
61.00
81.00
101.00
121.00
141.00
161.00
181.00

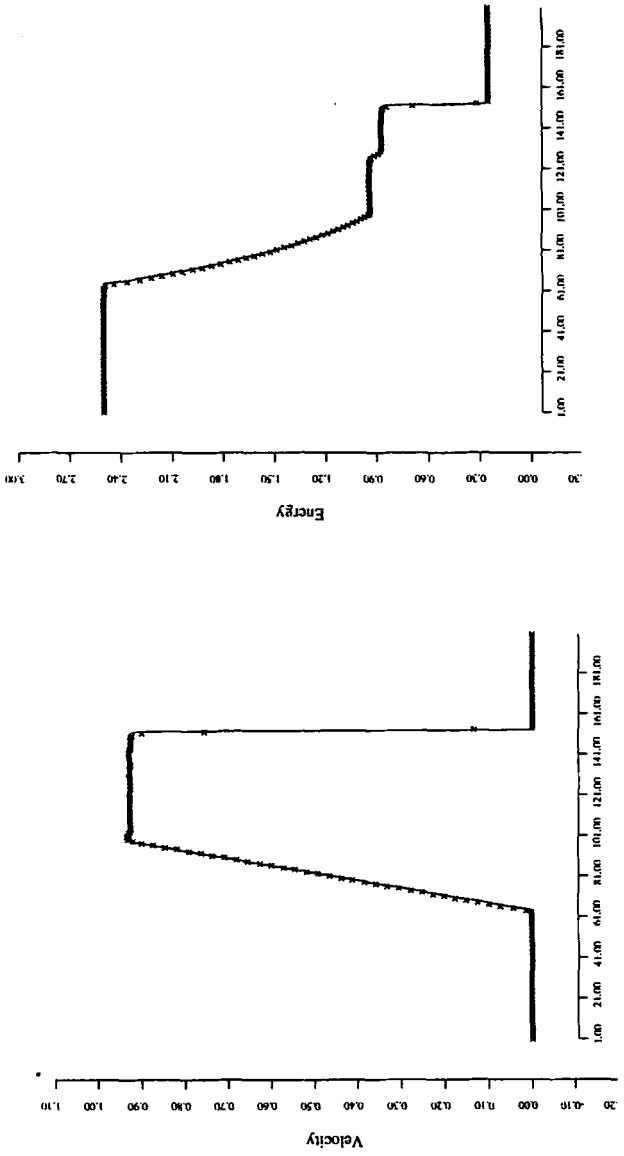

Fig. 1. Sod test case with 200 cells.

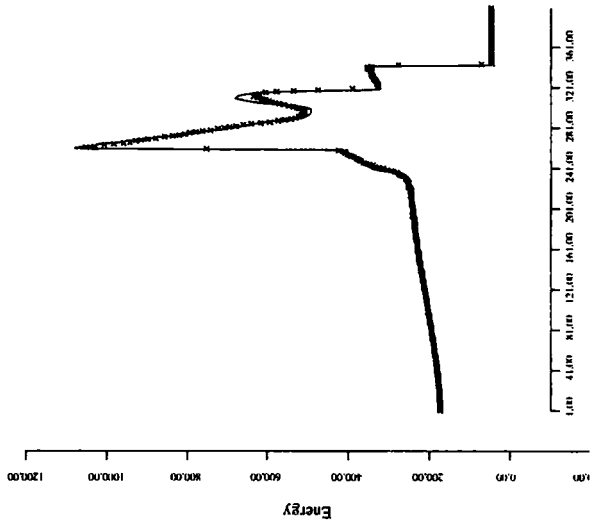
Energy
0.00
200.00
400.00
600.00
800.00
1000.00
1200.00
1.00
41.00
81.00
121.00
161.00
201.00
241.00
281.00
321.00
361.00

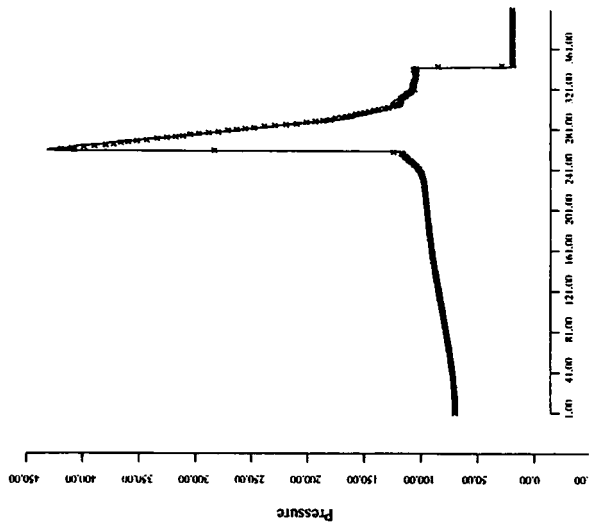
Pressure
0.00
50.00
100.00
150.00
200.00
250.00
300.00
350.00
400.00
450.00
1.00
41.00
81.00
121.00
161.00
201.00
241.00
281.00
321.00
361.00

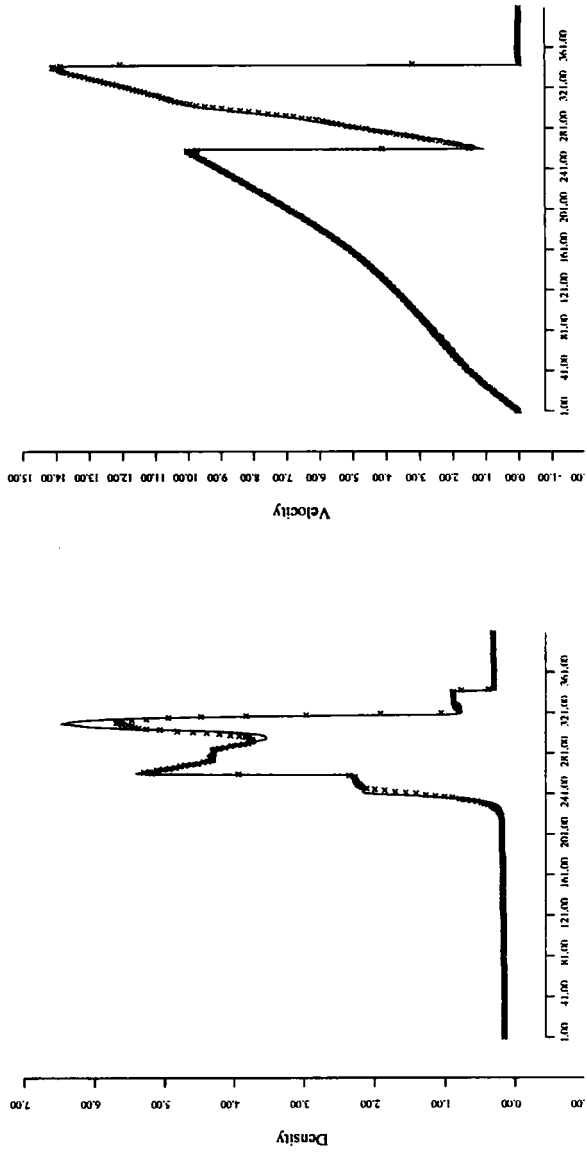

Fig. 2. Blast-wave test case with 400 cells.

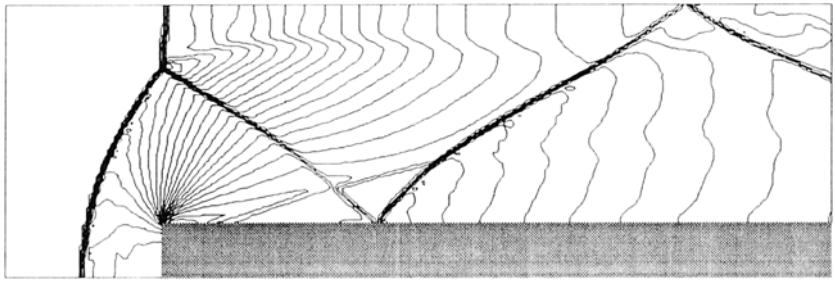

Fig. 3. Density distribution for Mach 3 wind tunnel test with 240×80 cells.

Case 4. The Mach 10 reflection of a strong shock test is calculated on the computational domain of 360×120 cells.[19] The problem is set up by driving a shock down a tube which contains a wedge. The density distribution after the collision between the shock and the wedge is shown in Fig. 4.

All these results confirm the accuracy and high resolution of the current gas-kinetic relaxation scheme. Complex features, such as oblique shocks and the triple points, are captured without oscillations. $\mathscr{L}(\cdot)$ controls both the numerical and physical dissipation in the current scheme, and we cannot say that the optimal choice of $\mathscr{L}(\cdot)$ has been obtained in this paper.

4. CONCLUSION

The gas-kinetic relaxation scheme presented in this paper is a simplified version of the schemes developed in the earlier papers from the solution of the gas-kinetic BGK model. This new scheme provides a gas-dynamical model to account for the time evolution of the gas distribu-

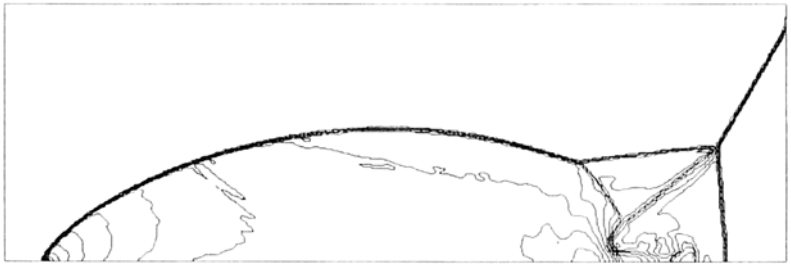

Fig. 4. Density distribution for double shock reflection test on mesh 360×120.

tion function starting from a cell boundary. The initial condition used here is more flexible than those used in the Godunov-type schemes. Also, the final gas distribution function combines both the gas-kinetic Lax–Wendroff and upwind schemes, while the nonequilibrium and equilibrium states are coupled according to the local physical situation. Due to the freedom in constructing the microscopic dynamical models of a gas flow, a host of variations of the present scheme can be obtained by justifying the relaxation parameter $\mathscr{L}(\cdot)$. Actually, the problem is still solvable by the inclusion of more space and time variation terms, such as $x^2, y^2, xy, xt,...$, in g and f_0 for the multidimensional flow simulations. As we know, a multidimensional scheme should have multidimensional properties in both the interpolation and dynamical evolution stages. Breaking through the limitation of the Godunov-type schemes, the methods based on the BGK model capture naturally a multidimensional gas evolution processes. One of the most important point in this paper is to point out that gas-kinetic schemes are not about the study of the motion of individual particles at a microscopic level. In fact, after the moment integrations, no microscopic variables appear in our final fluxes in the present scheme, and the time steps used for all test cases in the numerical part are CFL time steps. Many people who are not familiar with the literature misunderstand or misjudge gas-kinetic schemes. They still cling to the traditional ideas about gas kinetics, that gas kinetics only concerns the study of the details of the microscopic phenomena and is not of much help for macroscopic flow simulations. The current paper, along with the previous ones,[12, 21, 22] shows that efficient numerical schemes can be constructed in a gas-kinetic way without getting into the details of the particle collisions. Actually, as shown in this paper, the unification of mass, momentum, and energy and their fluxes into a single gas distribution function with explicit expression makes the scheme simpler than many other schemes currently used, especially for multidimensional calculations. The numerical results for many test cases demonstrate that this class of new methods is competitive with other high-resolution shock-capturing schemes.

REFERENCES

1. P. L. Bhatnagar, E. P. Gross, and M. Krook, *Phys. Rev.* **94**:511 (1954).
2. P. Colella and P. Woodward, The piecewise parabolic method (PPM) for gas-dynamical simulations, *J. Comput. Phys.* **54**:174 (1984).
3. S. K. Godunov, A difference scheme for numerical computation of discontinuous solutions of hydrodynamic equations, *Math. Sbornik* **47**:271 (1959).
4. A. Harten, On a class of high resolution total variation stable finite difference schemes, *SIAM J. Numerical Anal.* **21**:1-23 (1984).
5. A. Harten, B. Engquist, S. Osher, and S. Chakravarthy, Uniformly high order accurate essentially non-oscillatory schemes, III, *J. Comput. Phys.* **71**: 231–303 (1987).

6. A. Jameson, Artificial diffusion, upwind biasing, limiters and their effect on accuracy and multigrid convergence in transonic and hypersonic flows, AIAA paper 93-3359 (1993).
7. A. Jameson, Analysis and design of numerical schemes for gas dynamics 1. Artificial diffusion, upwind biasing, limiters and their effect on accuracy and multigrid convergence, *Int. J. Computational Fluid Dynam.*, submitted (1994).
8. A. Jameson, W. Schmidt, and E. Turkel, Numerical solutions of the Euler equations by finite volume methods using Runge-Kutta time-stepping schemes, AIAA paper 81–1259 (1981).
9. M. N. Kogan, *Rarefied Gas Dynamics* (Plenum Press, New York, 1969).
10. M.-S. Liou and C. J. Steffen, A new flux splitting scheme, NASA-TM 104452 (1991).
11. J. C. Mandal and S. M. Deshpande, Kinetic flux vector splitting for euler equations, *Computers Fluids* **23**(2):447 (1994).
12. K. H. Prendergast and K. Xu, Numerical hydrodynamics form gas-kinetic theory, *J. Comput. Phys.* **109**:53 (1993).
13. P. L. Roe, Approximate Riemann solvers, parameter vectors and difference schemes, *J. Comput. Phys.* **43**: 357 (1981).
14. G. A. Sod, A survey of several finite difference methods for systems of nonlinear hyperbolic conservation laws, *J. Comput. Phys.* **27**:1–31 (1978).
15. J. L. Steger and R. F. Warming, Flux vector splitting of the inviscid gas-dynamic equations with applications to finite difference methods, *J. Comput. Phys.* **40**:263–293 (1981).
16. B. van Leer, Flux-vector splitting for the Euler equations, ICASE report, No. 82-30 (September 1982).
17. B. van Leer, Upwind-difference methods for aerodynamic problems governed by the Euler equations, in *Large-Scale Computations in Fluid Mechanics*, B. E. Engquist, S. Osher, and R. Somerville, eds. (1985).
18. M. Vinokur, An analysis of finite-difference and finite-volume formulations of conservation laws, *J. Comput. Phys.* **81**:1–52 (1989).
19. P. Woodward and P. Colella, Numerical simulations of two-dimensional fluid flow with strong shocks, *J. Comput. Phys.* **54**:115 (1984).
20. K. Xu, Numerical hydrodynamics from gas-kinetic theory, Ph.D. thesis, Columbia University (1993).
21. K. Xu and K. H. Prendergast, Numerical Navier–Stokes solutions from gas-kinetic theory, *J. Comput. Phys* **114**: 9–17 (1994).
22. K. Xu, L. Martinelli, and A. Jameson, Gas-kinetic finite volume methods, flux-vector splitting and artificial diffusion, *J. Comput. Phys.* **120**:48–65 (1995).